Radiation Pattern Computation of Cavity-Backed and Probe-Fed Stacked Microstrip Patch Arrays

Miguel A. González de Aza, José A. Encinar, *Member, IEEE*, and Juan Zapata, *Member, IEEE*

***Abstract*—In this paper, two different methods based on the Floquet's harmonic expansion of the electromagnetic field in half-space are proposed to determine the active element pattern of infinite planar arrays. They allow us to obtain the radiating characteristics without the limitations of the conventional method from the active reflection coefficient. Both are applied to analyze the scan performance in the case of probe-fed and cavity-backed microstrip arrays from its generalized scattering matrix (GSM), computed previously with a full wave numerical procedure. Numerical results are presented and compared with other techniques.**

***Index Terms*—Antenna radiation patterns, finite-element methods, microstrip arrays, scattering matrices.**

I. Introduction

ONE of the fundamental characteristics of the phased-array antennas is the variation of gain and input impedance when the array is scanned. It is well known [1] that the interaction between array elements makes these parameters depend on the feeding phase shifts and, therefore, the principle of pattern multiplication from the isolated element and the array factor is not applicable. A usual way to characterize the scan performance in phased arrays is the active element pattern, which is defined as the field pattern radiated by an array when one element is excited and all the others are terminated in matched loads [2]. The active element pattern will be different for each element in a finite array owing to a different mutual coupling. However, in the case of finite but large arrays the behavior of all the elements is almost equal and it is possible to neglect the edge effects and to apply the infinite array approach. Therefore, the active element pattern is the same for all the radiating elements and the superposition theorem may be applied from the active element pattern and the array factor. All the mutual coupling effects are implicitly taken into account. The practical interest of the active element pattern lies in the fact that it is proportional to the gain of the array at a given scan angle [2] and it is relatively easy to measure with only one excited element. In practice, it provides a good estimation of the gain pattern for finite arrays even with few elements.

For infinite arrays, the normalized active element power pattern is frequently obtained from the active reflection coefficient, which can be related intuitively applying power conservation considerations [2] or using scattering parameters [3]. However, this technique has several restrictions since it is valid only when losses are not present in the structure, it provides only power patterns and no information can be obtained on field patterns or cross-polarization levels. Besides, this expression is not valid when grating lobes are present in the visible range since there is no way to discern the power going to the main lobe from the grating lobe power. A method to compute the active element pattern that overcomes all these drawbacks is proposed in [4]. In this reference, the active element pattern is derived from the current distribution on the patch, which is obtained by the integral equation and Green's function formalisms.

On the other hand, stacked microstrip patches with several dielectric layers are used to improve the bandwidth, gain, or efficiency antenna performance or to operate in dual frequency. The insertion of metallic walls between the patch elements also has been considered in the last years to prevent surface wave modes. This configuration allows to utilize thick substrates in order to increase the impedance bandwidth of the antenna without the limitation in the scanning range or even to achieve a considerable improvement in scan performance [5]. To analyze multilayer structures, full wave efficient numerical methods based on modular approaches have been proposed [6]–[8]. In these techniques, each interface or transition, including the feeding, is considered as a building block and it characterized by a generalized scattering matrix (GSM). Multilayer structures are analyzed with a modular approach in a more flexible and efficient way that with an integrated approach since modifications on one layer only require a single GSM calculation and not a whole recomputation.

In this work, two procedures are proposed to compute the active element power and field patterns in infinite planar arrays. They are deduced from the Floquet's harmonic representation of the electromagnetic field generated by the array and they are applicable when grating lobes and losses are present. The active element patterns are directly computed from the GSM which characterizes the array. The methods are applied to obtain the radiation characteristics of probe-fed and multilayer microstrip arrays of patches in single and stacked configurations and backed by metallic cavities, analyzed previously with the modular procedure proposed in [6]. Active element patterns for several arrays and comparisons with other numerical predictions are presented.

II. Method I: Active Element Pattern Computed from Floquet's Harmonics

In this section, an accurate relation to obtain the field and power active element patterns in infinite planar arrays is derived. The procedure is parallel to the method presented in [4]

Manuscript received November 12, 1998; revised October 20, 1999. This work was supported by the Spanish "Comisión Interministerial de Ciencia y Tecnología" (CICYT) under Project TIC98-0929-C02-01.

The authors are with the Departamento de Electromagnetismo y Teoría de Circuitos, ESTI of Telecommunications, Universidad Politécnica de Madrid, Madrid, 28040 Spain.

Publisher Item Identifier S 0018-926X(00)03241-5.

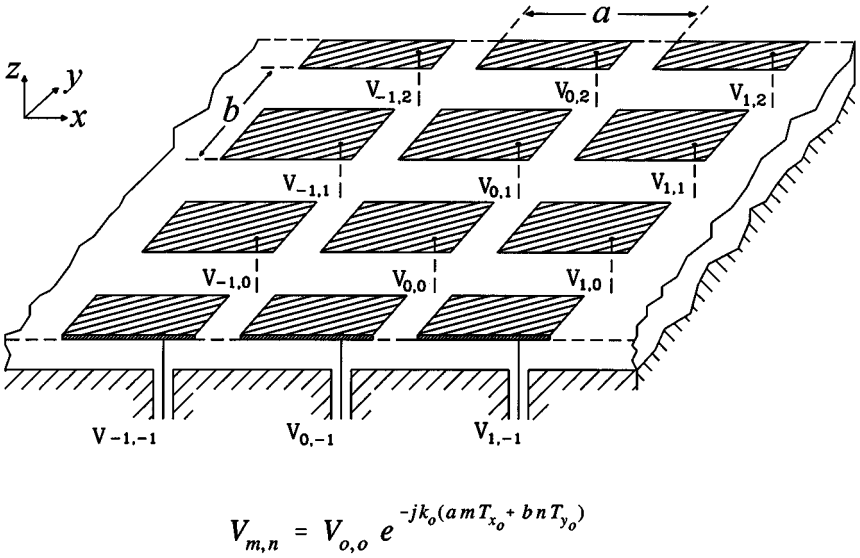

Fig. 1. Conventional infinite planar microstrip phased array of probe-fed rectangular microstrip patches with a same amplitude and a linear phase shift excitation given by $V_{m,n}$.

from the Green's function but based on the identification with Floquet's harmonics. Let us consider an infinite phased planar array with a rectangular periodicity $a \times b$, all cells with an identical amplitude excitation voltage, and a linear phase shift defined by (T_{x_o}, T_{y_o}) in the x and y directions, respectively. Fig. 1 shows a case of a conventional microstrip patch array probe fed via an inner conductor of coaxial transmission line. Next, the total far-field radiated by the array scanned toward the direction (θ_o, φ_o) is expressed in two ways. On the one hand, the total electromagnetic field over a periodic planar array with a linear phase shift excitation may be represented using a Floquet's harmonic expansion [1]. The electric field in the half-space (region $z > 0$ in Fig. 1) may be written as a summation of TE (h) and TM (e) space harmonics

$$\vec{E}_T = \sum_{l=1}^{\infty} \left[a_l^h \vec{e}_l^{\,h}(k_{xl}, k_{yl}) + a_l^e \vec{e}_l^{\,e}(k_{xl}, k_{yl})\right] \times e^{jk_{xl}x} e^{jk_{yl}y} e^{-jk_{zl}z} \tag{1}$$

where

$$\vec{e}_l^{\,h}(k_{xl}, k_{yl}) = \frac{1}{\sqrt{k_{xl}^2 + k_{yl}^2}}(-k_{yl}\hat{x} + k_{xl}\hat{y}) \quad \text{(TE)}$$
$$\vec{e}_l^{\,e}(k_{xl}, k_{yl}) = \frac{1}{\sqrt{k_{xl}^2 + k_{yl}^2}}(k_{xl}\hat{x} + k_{yl}\hat{y} + E_{zl}\hat{z}) \quad \text{(TM)}. \tag{2}$$

a_l^h and a_l^e are the complex coefficients of the lth Floquet harmonic and k_{xl}, k_{yl} and k_{zl} are the components of the propagation vector given by

$$k_{xl} = k_{xm} = \frac{2m\pi}{a} - k_o \sin\theta_o \cos\varphi_o$$
$$k_{yl} = k_{yn} = \frac{2n\pi}{b} - k_o \sin\theta_o \sin\varphi_o$$
$$k_{zl} = k_{zm,n} = \sqrt{k_o^2 - k_{xl}^2 - k_{yl}^2}. \tag{3}$$

The two indexes m and n are reduced to one l by ordering the Floquet's harmonics as the cutoff frequency increases. The z-component of the electric field for TM harmonics is obtained directly from the plane wave relations. (θ_o, φ_o) coincides with the radiated plane wave direction corresponding to the fundamental space harmonic ($m = n = 0$ or $l = 1$).

On the other hand, the radiated field is the superposition of the active element field $\vec{E}_e(r, \theta, \varphi)$, which is written by separating the spherical wave variation with the r-coordinate and the array factor (AF)

$$\vec{E}_T(r, \theta, \varphi) = \vec{E}_e(\theta, \varphi)\frac{e^{-jkr}}{r} \cdot \mathrm{AF}(\theta, \varphi) \tag{4}$$

where

$$\mathrm{AF}(\theta, \varphi) = \sum_{m=-\infty}^{\infty} \sum_{n=-\infty}^{\infty} e^{jmak_o(T_x - T_{x_o})} e^{jnbk_o(T_y - T_{y_o})} \tag{5}$$

$$T_x = \sin\theta\cos\varphi \quad T_{x_o} = \sin\theta_o \cos\varphi_o$$
$$T_y = \sin\theta\sin\varphi \quad T_{y_o} = \sin\theta_o \sin\varphi_o$$

and k_o is the free-space wave number.

If the array factor is expressed in (4) as a double summation of Dirac-delta functions, the spherical wave as a plane wave spectrum and after the calculation of the resultant integral, the right-hand side of the equation results in

$$\vec{E}_T(r, \theta, \varphi) = \vec{E}_e(\theta, \varphi)\frac{2\pi}{ab} \cdot \sum_{m=-\infty}^{\infty} \sum_{n=-\infty}^{\infty} \frac{e^{-jk_{zm,n}z}}{k_{zm,n}} e^{jk_{xm}x} e^{jk_{yn}y} \tag{6}$$

where k_{xm}, k_{yn} and $k_{zm,n}$ are defined in (3). This expression corresponds with a summation of homogeneous and evanescent

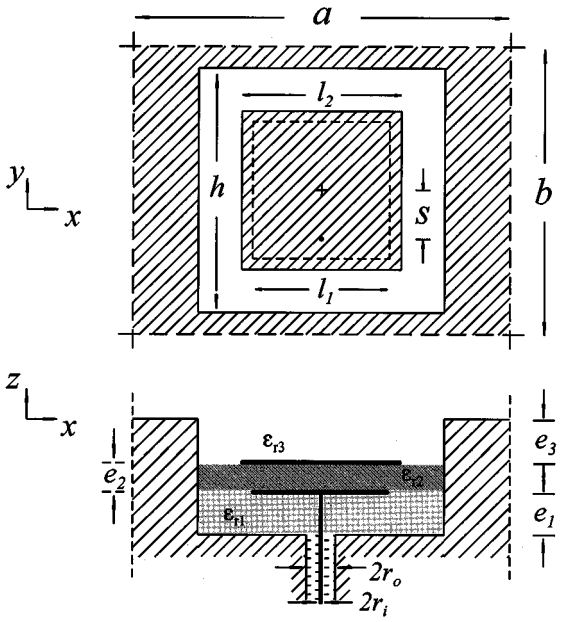

Fig. 2. Elementary cell of an infinite array of stacked cavity-backed square patches fed by coaxial lines. ($l_1 = 1.35$ cm; $l_2 = 1.458$ cm; $h = 1.815$ cm; $s = 1.75$ mm; $a = 2.378$ cm; $b = 2.215$ cm; $e_1 = 2.42$ mm; $e_2 = 1.5$ mm; $e_3 = 2.0$ mm; $\varepsilon_{r1} = 2.61$; $\varepsilon_{r2} = 4.0$; $\varepsilon_{r3} = 1.0$; Coaxial feed: $\varepsilon_{rx} = 1.951$; $r_i = 0.64$ mm; $r_o = 2.05$ mm.)

space harmonics, which is expected from an infinite array under the applied excitation. By ordering the harmonics as the cutoff frequency increases and reducing the two indexes m and n to one l (6) results in

$$\vec{E}_T(r,\theta,\varphi) = \vec{E}_e(\theta,\varphi)\frac{2\pi}{ab}\cdot\sum_{l=L}^{\infty}\frac{e^{-jk_{zl}z}}{k_{zl}}e^{jk_{xl}x}e^{jk_{yl}y}. \quad (7)$$

Taking the element pattern function inside the summation sign, the total far field radiated may be expressed as

$$\vec{E}_T(r,\theta,\varphi) = \frac{2\pi}{ab}\cdot\sum_{l=1}^{\infty}\vec{E}_e(\theta_l,\varphi_l)\frac{e^{-jk_{zl}z}}{k_{zl}}e^{jk_{xl}x}e^{jk_{yl}y}. \quad (8)$$

Identifying expressions (8) and (1) the following relationship is obtained for each term of the summation, including both propagating and evanescent harmonics:

$$\left[a_l^h\vec{e}_l^{\,h}(k_{xl},k_{yl}) + a_l^e\vec{e}_l^{\,e}(k_{xl},k_{yl})\right]e^{jk_{xl}x}e^{jk_{yl}y}e^{-jk_{zl}z} = \frac{2\pi}{ab}\cdot\vec{E}_e(\theta_l,\varphi_l)\frac{e^{-jk_{zl}z}}{k_{zl}}e^{jk_{xl}x}e^{jk_{yl}y}. \quad (9)$$

Finally, the active element field pattern without the space factor and corresponding to the main lobe scanned to (θ_o,φ_o) is obtained for $l = 1$

$$\vec{E}_e(\theta_o,\varphi_o) = \frac{ab}{2\pi}k_{z1}\left[a_1^h\vec{e}_1^{\,h}(k_{x1},k_{y1}) + a_1^e\vec{e}_1^{\,e}(k_{x1},k_{y1})\right]. \quad (10)$$

a_1^h and a_1^e are the complex coefficients of the TE and TM components corresponding to the first Floquet harmonic $(m = 0, n = 0)$ and will vary with the scanning angle. Taking into account (2) and (3) for the first harmonic and the relation between Cartesian and spherical unit vectors, we obtain the active element field pattern in spherical coordinates

$$\vec{E}_e(\theta,\varphi) = \frac{ab}{2\pi}k_o\left[\cos\theta a_1^h(\theta,\varphi)\hat{\varphi} + a_1^e(\theta,\varphi)\hat{\theta}\right]. \quad (11)$$

This expression provides field radiation patterns in a rigorous way, is applicable when losses are included in the computation, and when grating lobes are present. In such a case, also an identification from (9) can be done to yield an expression similar to (11) for higher order harmonics.

This technique is directly applicable in the analysis of probe-fed and multilayered infinite arrays of cavity-backed microstrip patches in single or stacked configuration from the space harmonics calculated previously with the full wave method presented in [6]. Fig. 2 shows the unit cell of an array of this type with square patches. The quoted procedure combines the mode-matching (MM) GSM techniques and the two-dimensional finite-element method (2-D FEM), and it is based on the consideration of the elementary cell as an open-ended succession of homogeneous waveguides of diverse cross sections (multistepped structure), with the same direction of propagation (z axis in Fig. 2) radiating into half-space. The radiated field is expressed as a Floquet's harmonic expansion and a modal representation, either analytical or numerical, is used in the homogeneous waveguides. Each transition between waveguides and the interface between the infinite array of apertures and the free half-space are solved by the MM technique to obtain their individual GSM. A hybrid MM-FEM procedure is used for the analysis of discontinuities that involve homogeneous waveguides of arbitrary cross section. A cascade connection process for the GSM's of the waveguide discontinuities and the aperture provides the GSM that characterizes the array

$$\begin{bmatrix}B\\A\end{bmatrix} = \begin{bmatrix}S_{11} & S_{12}\\S_{21} & S_{22}\end{bmatrix}\begin{bmatrix}D\\C\end{bmatrix} \quad (12)$$

which relates incident (D) and reflected (B) modes in the coaxial line and incident (C) and scattered (A) Floquet's harmonics in the half-space. The first element of the column matrix B is the amplitude of the TEM mode reflected in the coaxial line and A is the column matrix $[A] = \{a_1^h, a_2^h, \cdots, a_L^h, a_1^e, a_2^e, \cdots, a_L^e\}$, after the truncation of the harmonic expansion (1) required to implement the MM technique. Thus, if the array is excited by the TEM mode in the coaxial feed, which corresponds to $[D] = \{1, 0, \cdots, 0\}$ and $[C] = [0]$, the active reflection coefficient of the infinite array, $R(\theta,\varphi)$ and the space harmonics coefficients $a_1^h(\theta,\varphi)$ and $a_1^e(\theta,\varphi)$ from which the active element pattern is computed (11), are the element matrix $S_{11}(1,1), S_{21}(1,1)$ and $S_{21}(L+1,1)$ respectively. These coefficients and, therefore, the matrix (12) must be computed for each considered direction (θ,φ) in (11). However, the GSM that characterizes the multistepped waveguide structure without including the array of apertures half-space transition (see [6]) is computed once because this matrix is independent of the scanning angle. Only the GSM of the aperture problem will vary with the scanning angle.

III. Method II: Active Element Pattern from Aperture Theory and Floquet's Harmonics

In this section, the active element pattern is derived from the aperture theory and the space harmonic representation of the electromagnetic field on the array surface. The far field generated in $z \geq 0$ for an arbitrary aperture field situated in the $z = 0$ plane, calculated from the plane wave spectrum representation of electromagnetic fields [9], and using the stationary phase approximation is written as

$$\vec{E}(r,\theta,\varphi) = 2\pi jk[(\hat{\theta}\cos\varphi - \hat{\varphi}\sin\varphi\cos\theta)\tilde{E}_{ax}(\theta,\varphi) + (\hat{\theta}\sin\theta - \hat{\varphi}\cos\varphi\cos\theta)\tilde{E}_{ay}(\theta,\varphi)]\frac{e^{-jkr}}{r} \tag{13}$$

where $\tilde{E}_{ax}$ and $\tilde{E}_{ay}$ are the Cartesian components of the tangential electric field E_{ax} and E_{ay} in the spectral domain

$$\tilde{E}_{ax(y)}(k_x,k_y) = \int_{-\infty}^{\infty}\int_{-\infty}^{\infty} E_{ax(y)}(x,y)e^{j(k_x x + k_y y)}\,dx\,dy. \tag{14}$$

This approach rejects the contribution of the surface waves to the angular spectrum of plane waves in half-space and is applicable to points sufficiently separated from the $z = 0$ plane.

Equation (13) will be applicable to compute the radiated field of a planar array if the tangential electric field is known on the entire surface of the array. For a phased periodic array the tangential field in spectral domain, (14) may be written from the transformed field on a periodic cell as

$$\tilde{E}_{ax(y)}(k_x,k_y) = \mathrm{AF}\cdot\tilde{E}_{ex(y)}(k_x,k_y) \tag{15}$$

with

$$\tilde{E}_{ex(y)}(k_x,k_y) = \int\int_s E_{ax(y)}(x,y)e^{j(k_x x + k_y y)}\,dx\,dy \tag{16}$$

where s is the elementary cell surface. After replacing (15) in (13) and identifying this one with (4), the active element field pattern may be calculated as

$$\vec{E}_e(\theta,\varphi) = 2\pi jk[(\hat{\theta}\cos\varphi - \hat{\varphi}\sin\varphi\cos\theta)\tilde{E}_{ex}(\theta,\varphi) + (\hat{\theta}\sin\theta - \hat{\varphi}\cos\varphi\cos\theta)\tilde{E}_{ey}(\theta,\varphi)]. \tag{17}$$

On the other hand, we may obtain the tangential electromagnetic field over the surface of an infinite periodic phased array based on the Floquet's harmonic expansion by putting $z = 0$ in (1). Substituting (2) into the resultant expression and after some algebraic manipulations the tangential field components may be calculated as

$$E_{ax} = \sum_{l=1}^{\infty} d_{xl}e^{j(k_{xl}x + k_{yl}y)};\quad E_{ay} = \sum_{l=1}^{\infty} d_{yl}e^{j(k_{xl}x + k_{yl}y)} \tag{18}$$

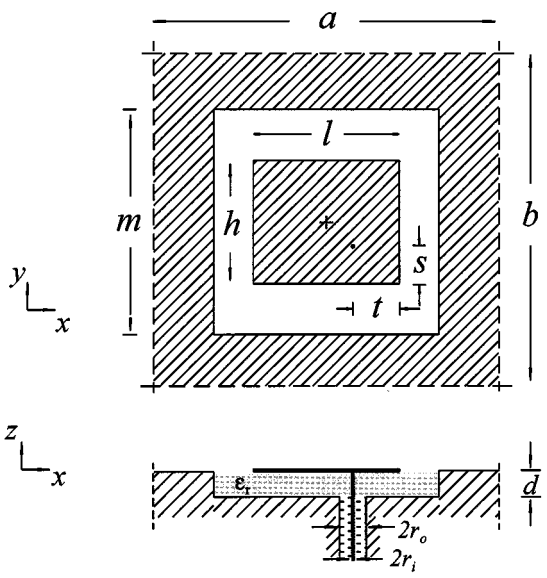

Fig. 3. Elementary cell of an infinite array of cavity backed rectangular patches in single configuration fed by probe-coaxial lines. ($a = b = 10$ cm; $l = 6$ cm; $h = 4$ cm; $m = 9.95$ cm; $s = t = 1$ cm; $\varepsilon_r = 4.32$; $d = 0.8$ mm; Coaxial feed: $\varepsilon_{rx} = 1.951$; $r_i = 0.64$ mm; $r_o = 2.05$ mm.)

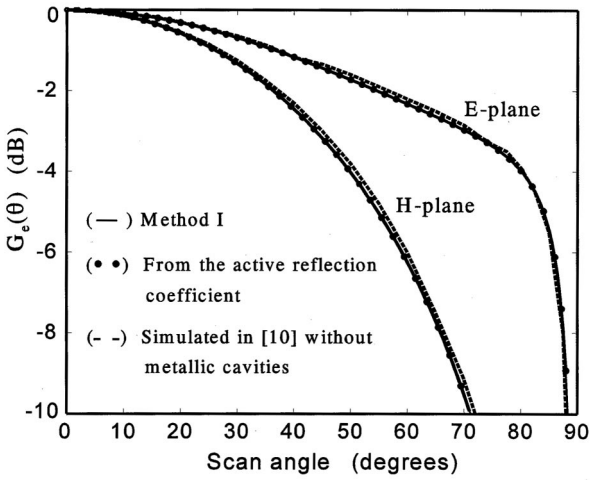

Fig. 4. Normalized active element pattern of the infinite array of rectangular microstrip patches defined in Fig. 3 computed from different methods, $f = 1.21$ GHz.

where

$$d_{xl} = \frac{-a_l^h k_{yl} + a_l^e k_{xl}}{\sqrt{k_{xl}^2 + k_{yl}^2}};\quad d_{yl} = \frac{a_l^h k_{xl} + a_l^e k_{yl}}{\sqrt{k_{xl}^2 + k_{yl}^2}}. \tag{19}$$

Finally, substituting (18) in (16), taking the integrals inside the summation sign, and after the integration over the elementary cell we obtain for an array with a rectangular periodicity

$$\tilde{E}_{ex(y)}(k_x,k_y) = 4\sum_{l=1}^{\infty}\left[d_{x(y)l}\frac{\sin[(k_x + k_{xl})a/2]}{(k_x + k_{xl})}\frac{\sin[(k_y + k_{yl})b/2]}{(k_y + k_{yl})}\right] \tag{20}$$

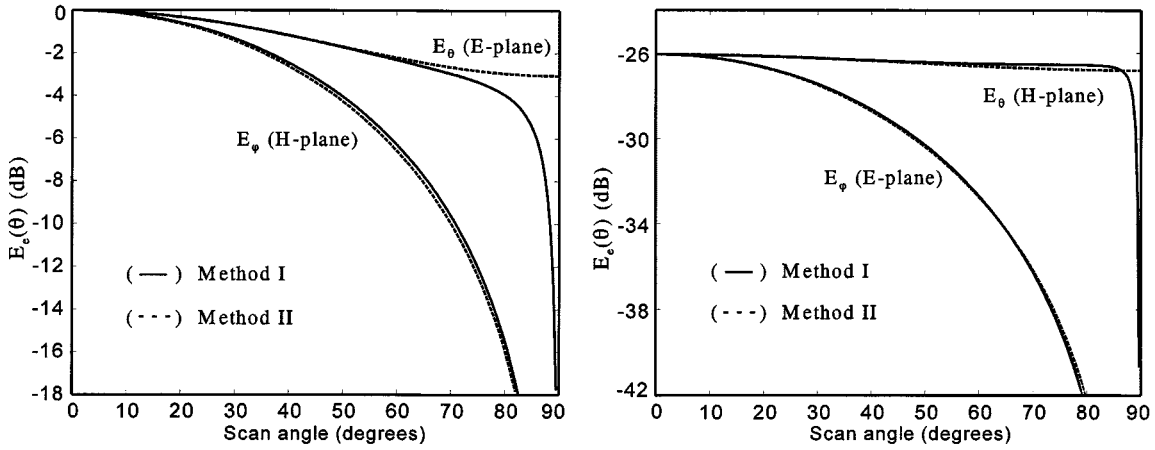

(a) (b)

Fig. 5. Normalized active element field pattern of the infinite array of rectangular microstrip patches defined in Fig. 3 computed from the methods I and II, $f = 1.21$ GHz. (a) Copolar component. (b) Cross-polar component.

which together with (17) provides the active element pattern from the Floquet's harmonic coefficients. In practice, the infinite summation in (20) must be truncated to a finite number of Floquet's harmonics. This technique also allows to obtain field and power radiation patterns when grating lobes and losses are present.

In the case of the analysis of cavity-backed microstrip patches from the method in [6], the coefficients a_l^h and a_l^e in (19) are obtained directly from the GSM that characterizes the array (12) as described in previous section. These coefficients may be computed at any angle (k_{xl}, k_{yl}) but only once. Therefore, this matrix and particularly the GSM of the aperture problem only must be computed once, saving computer time unlike the technique proposed in the previous section. However, (17) is obtained from the stationary phase approach and it is not applicable to points close to the array plane $(z = 0)$.

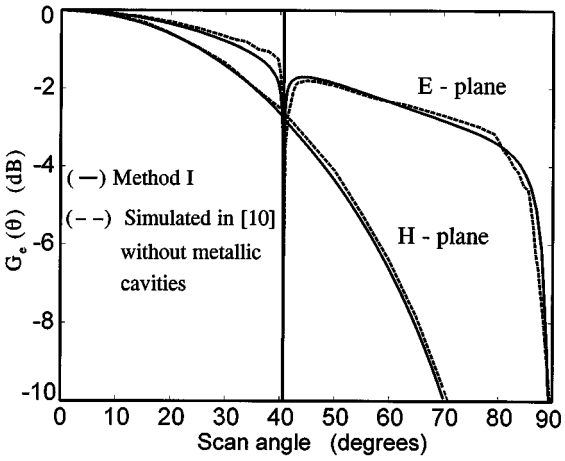

Fig. 6. Normalized active element pattern of the infinite array of rectangular microstrip patches defined in Fig. 3 with $a = b = 15$ cm., $f = 1.21$ GHz.

IV. Numerical Results

The preceding techniques are now applied to obtain the active element pattern of different probe-fed cavity backed microstrip arrays. Results from the proposed methods and comparisons with other numerical predictions are presented to evaluate their usefulness. The unit cell of the first considered array is depicted Fig. 3. The patch elements are fed by the center conductor of an SMA connector of 50 Ω. All the probe dimensions and the dielectric constant have rigorously been taken into account in the analysis method. Fig. 4 presents the active element pattern in E and H planes at the resonant frequency of 1.21 GHz computed from method I and from the active reflection coefficient with the known expression $G_e(\theta, \varphi) = (1 - |R(\theta, \varphi)|^2) \cos\theta$. This relation is applicable in this case since no grating lobes are present ($a = b = 0.4\lambda_o$ at the resonant frequency). Both methods lead to the same results since losses are not considered in the simulations. Moreover, the figure shows numerical results for the same array, analyzed in [10], but without metallic cavities (infinite substrate as shown in Fig. 1). A very good agreement with the results in the reference is observed. This comparison is possible since, as deduced from the analysis in [5] and also stated in [6], the scan performance of a conventional microstrip array on an infinite and thin substrate $d \leq 0.02\lambda_o$ is similar to the same array with metallic walls between the adjacent cells of the array. For the considered array the substrate thickness is $0.003\lambda_o$ at the resonant frequency. The E and H-plane active element field pattern of the copolar and cross-polar components are depicted in Fig. 5(a) and (b), respectively. Results computed with the method from the space harmonics (method I) and from the aperture field (method II) are compared. Both methods lead to identical results except for E_θ and scan angles close to endfire, because of the limitation in the stationary phase used in method II. As stated in Sections II and III, the GSM computation of the multistepped waveguide structure without the aperture problem is previous and common to the calculation of the AEP from both methods and independent of the scanning angle. The calculation of this matrix consumes 390 s central processing unit (CPU) time to obtain the curves in Fig. 5 on a 400-MHz Pentium II personal computer. This time will depend on the number of waveguide discontinuities (dielectric substrates, stacked patches), the number of nodes of the used meshes and the number modes

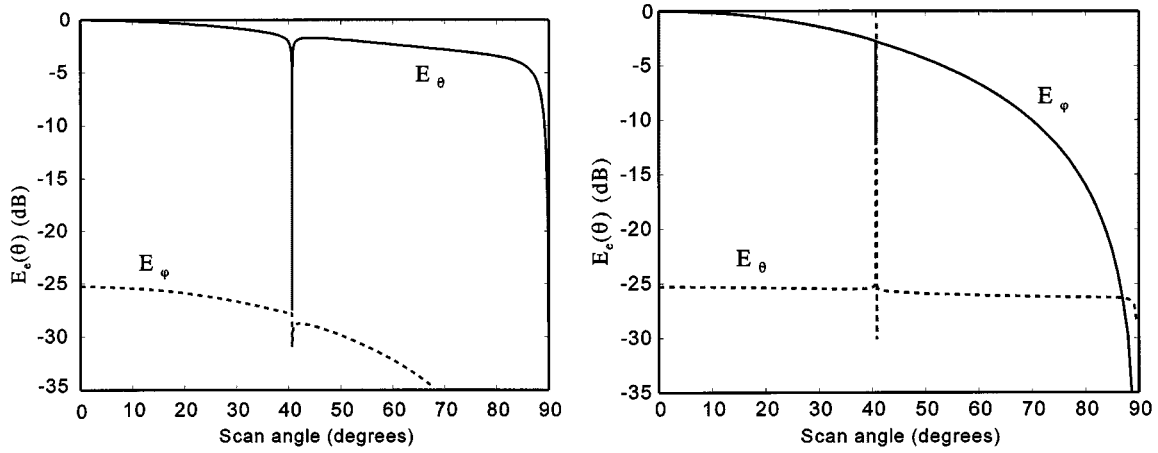

(a) (b)

Fig. 7. Normalized copolar and cross-polar active element pattern of the infinite array of rectangular microstrip patches defined in Fig. 3 with $a = b = 15$ cm, $f = 1.21$ GHz. (a) E-plane. (b) H-plane. Results obtained from the method I.

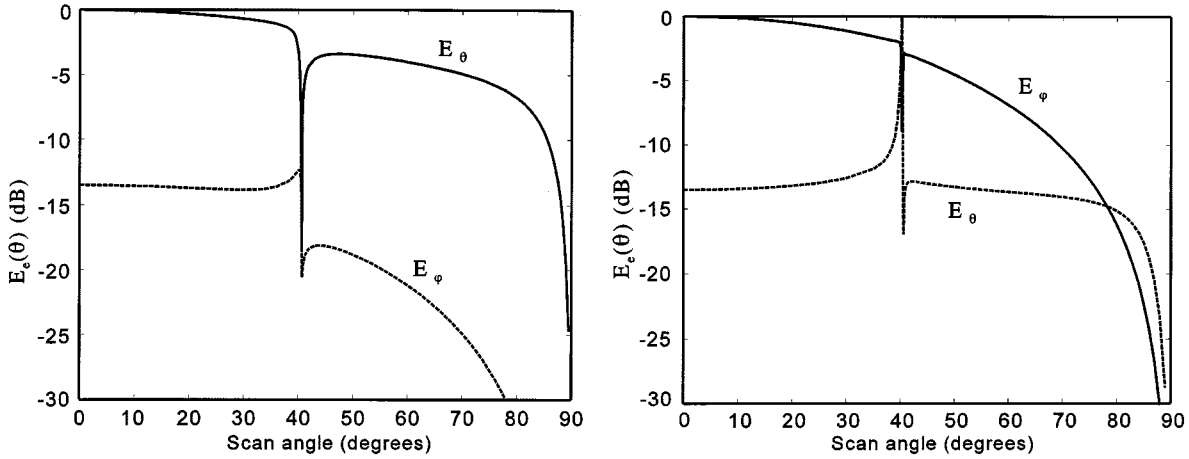

(a) (b)

Fig. 8. Normalized copolar and cross-polar active element pattern of the infinite array of rectangular microstrip patches defined in Fig. 3 with $a = b = 15$ cm and a substrate thickness $d = 1$ cm, $f = 1.21$ GHz. (a) E-plane. (b) H-plane. Results obtained from the method I.

needed to obtain convergent results as described and discussed in [6]. For the first method, nine more seconds for each additional scanning angle, consumed to solve the aperture problem are required using 114 TE plus 114 TM space harmonics. The second method from which the space harmonics are computed only once, requires 23 more seconds to obtain a whole curve. Therefore, to obtain the curve of Fig. 5 with 90 points, method I spends around three times the CPU time in method II. The required memory is similar for both methods.

In the second example, the same array is considered, but with a new element spacing larger than $\lambda_o/2$ ($a = b = 15$ cm $= 0.6\lambda_o$ at the resonant frequency of 1.21 GHz). Grating lobes and the scan blindness effect will appear. For the considered array, the appearance of the first grating lobe and the excitation of the first TM surface wave will occur practically at the same scan angle $(\theta = 40.7°)$ owing to the thin substrate thickness. In Fig. 6, the active element pattern in E and H planes computed with the first method proposed here are compared with the results in [10] for the same array without metallic cavities. A good concordance is observed between both predictions except at 40.7°. This fact is explained in Fig. 7 where the predicted co and crosspolar components are depicted. The curves show that taking a sufficient number of points in the axis corresponding to the scan angle, a blind spot also appears in the H plane at 40.7°, and the cross polar component is considerably incremented at the same scanning angle. In the case of cavity-backed patches the coupling due to the excitation of a surface wave of the dielectric slab is suppressed and the blindness coincides here with the appearance of the first grating lobe. In Fig. 8, results for the same array with a new substrate thickness $d = 1$ cm $= 0.04\lambda_o$ are plotted. The position of the blind spot (copolar components) remains at the same angle in spite of the thick substrate. For the same array with a conventional infinite substrate, a displacement of this one toward broadside may be expected.

As a third example, the stacked cavity-backed microstrip array with the unit cell given in Fig. 2 is considered. Fig. 9

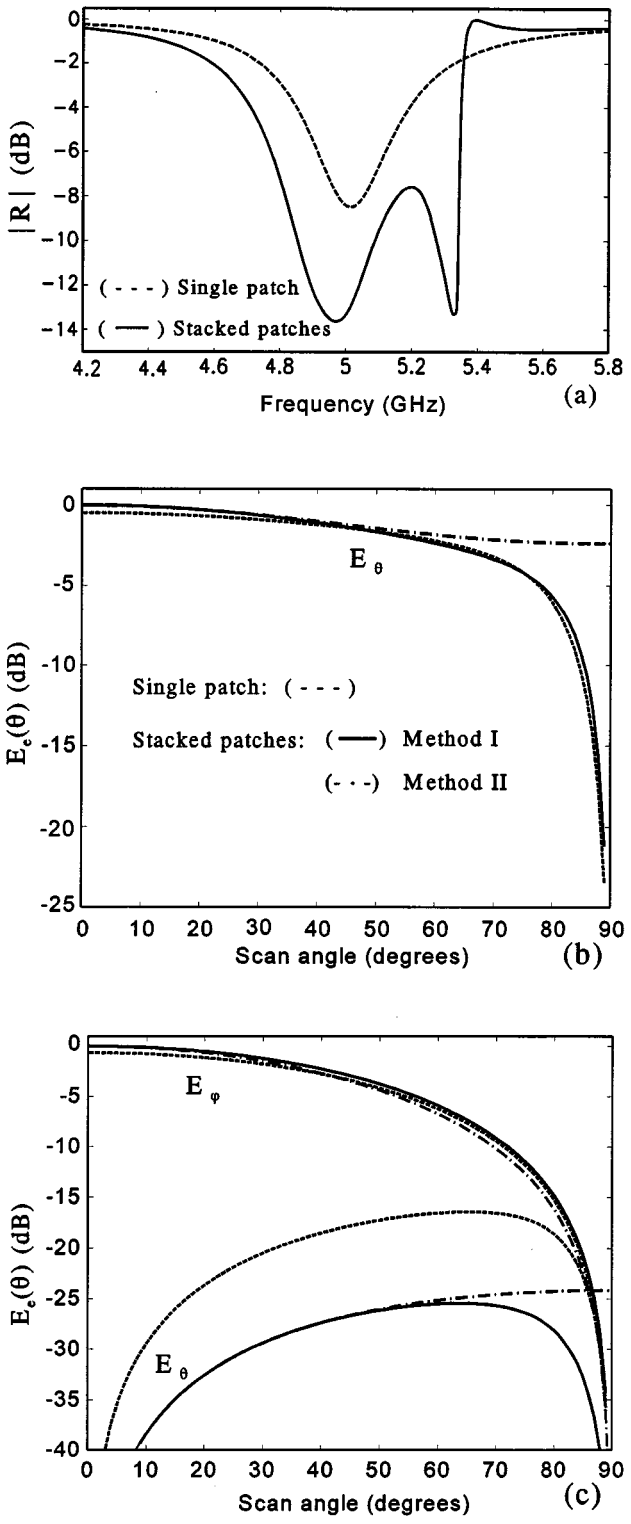

Fig. 9. (a) Broadside active reflection coefficient magnitude versus [(b) and (c)] frequency and normalized copolar and cross-polar active element pattern in E and H planes of the infinite array of rectangular microstrip patches defined in Fig. 2 in single and stacked patch configurations $f = 5.0$ GHz. (In the single patch design, the upper patch is suppressed and $e_3 = 0$.)

shows the broadside active reflection coefficient versus frequency and the active element field pattern for E and H planes computed by the methods I and II. As in the former case of single patches, both methods lead to similar results except for angles close to endfire. The E-plane cross-polarization component is almost zero. The CPU time consumed to solve the multistepped waveguide structure is 480 s in this case. From the first method, 11 more seconds for each additional scanning angle are required using 178 TE plus 178 TM space harmonics, whereas the method II only requires 35 more seconds to obtain a whole curve in Fig. 9. The same array in a single patch configuration (upper patch suppressed and $e_3 = 0$) is also analyzed. A bandwidth enhancement and a reduction of the crosspolarization level in the H plane are achieved with the stacked configuration.

V. Conclusion

Two efficient methods to compute the active element pattern of infinite phased arrays have been presented. They have been applied to obtain field and power radiating patterns of cavity-backed and probe-fed microstrip arrays. In both cases, the active element patterns are computed from the amplitudes of the Floquet's harmonics when the array is excited by the TEM mode in the coaxial feed. These amplitudes are a column of the GSM that characterizes the array. Since the modular approach based on the cascading of GSM's is very flexible for the analysis of multilayer arrays, both methods proposed here are very appropriated to compute the active element patterns and to analyze the scanning performance of such printed arrays. A good agreement has been obtained between both methods and with other numerical predictions, except for the method II at angles close to enfire owing to the stationary phase approximation. However, this method requires appreciably less computer time since the GSM computation of the aperture array is accomplished once in contrast to the first proposed method.

References

[1] N. Amitay, V. Galindo, and C. P. Wu, *Theory and Analysis of Phased Array Antennas*. New York: Wiley, 1972.

[2] R. C. Hansen, Ed., *Microwave Scanning Antennas—Volume II: Arrays Theory and Practice*. New York: Academic, 1966, vol. II.

[3] D. M. Pozar, "The active element pattern," *IEEE Trans. Antennas Propagat.*, vol. 42, pp. 1176–1178, Aug. 1994.

[4] A. K. Skrivervik and J. R. Mosig, "Analysis of finite phased array of microstrip patches," *IEEE Trans. Antennas Propagat.*, vol. 41, pp. 1105–1113, Aug. 1993.

[5] F. Zavosh and J. T. Aberle, "Infinite phased arrays of cavity-backed patches," *IEEE Trans. Antennas Propagat.*, vol. 42, pp. 390–398, Mar. 1994.

[6] M. A. González, J. A. Encinar, J. Zapata, and M. Lambea, "Full wave analysis of cavity-backed and probe-fed microstrip patch arrays by a hybrid mode-matching, generalized scattering matrix and finite-element method," *IEEE Trans. Antennas Propagat.*, vol. 46, pp. 236–242, Feb. 1998.

[7] J. A. Encinar, P. Gay-Balmaz, and J. R. Mosig, "Generalized scattering matrix computation of the transition microstrip line-array of arbitrarily shaped apertures—Application to the analysis of multilayer printed arrays," *10e J. Int. Nice Antennas, JINA '98*, vol. 1, pp. 33–36, 1998.

[8] A. K. Bhattacharyya, "A numerical model for multilayered microstrip phased-array antennas," *IEEE Trans. Antennas Propagat.*, vol. A44, pp. 1386–1393, Oct. 1996.

[9] R. H. Clarke and J. Brown, *Difraccion Theory on Antennas*. London, U.K.: Ellis Horwood, 1981.

[10] A. K. Skrivervik and J. R. Mosig, "Finite phased array of microstrip patch antennas: The infinite array approach," *IEEE Trans. Antennas Propagat.*, vol. 40, pp. 579–592, May 1992.

Miguel A. González de Aza was born in Madrid, Spain. He received the "Ingeniero de Telecomunicación" and Ph.D. degrees, both from the "Universidad Politécnica de Madrid," Spain, in 1989 and 1997, respectively.

From 1990 to 1992, he was with the Departamento de Electromagnetismo y Teoría de Circuitos, Universidad Politécnica de Madrid, with a research scholarship of the Spanish Ministry of Education and Science. He became Assistant Professor in 1992 and Associate Professor in 1997, at the same university. His main research interests include analytical and numerical techniques for the analysis and characterization of waveguide structures and microstrip antennas.

José A. Encinar (S'81–M'86) was born in Madrid, Spain. He received the Electrical Engineer and Ph.D. degrees, both from Universidad Politécnica de Madrid (UPM), Spain, in 1979 and 1985, respectively.

Since January 1980, has been with the Applied Electromagnetism and Microwaves Group, UPM, as a Teaching and Research Assistant from 1980 to 1982, an Assistant Professor from 1983 to 1986, and an Associate Professor from 1986 to 1991. From February through October of 1987 he was with the Polytechnic University, Brooklyn, NY, as a Postdoctoral Fellow of the NATO Science Program. Since 1991 he has been a Professor of the Electromagnetism and Circuit Theory Department, UPM. In 1996 he was with the Laboratory of Electromagnetics and Acoustics, Ecole Polytechnique Fédérale de Lausanne (EPFL), Switzerland, as Visiting Professor. His research interests include analytical and numerical techniques for the analysis and design of waveguide structures, frequency selective surfaces, and multilayer printed arrays.

Juan Zapata (M'93) received the "Ingeniero de Telecomunicación" and Ph.D. degrees, both from the "Universidad Politécnica de Madrid," Spain, in 1970 and 1974, respectively.

Since 1970, he has been with the Departamento de Electromagnetismo y Teoría de Circuitos, Universidad Politécnica de Madrid, where he became an Assistant Professor in 1970, an Associate Professor in 1975, and a Professor in 1983. He has been engaged in research on microwave active circuits and interactions of electromagnetic fields with biological tissues. His current research interest include computer-aided design for microwave passive circuits and numerical methods in electromagnetism.